Mon. Not. R. Astron. Soc. **370,** 884–890 (2006) doi:10.1111/j.1365-2966.2006.10526.x

Orbital elements, masses and distance of λ Scorpii A and B determined with the Sydney University Stellar Interferometer and high-resolution spectroscopy

W. J. Tango,[1⋆] J. Davis,[1] M. J. Ireland,[2] C. Aerts,[3,4] K. Uytterhoeven,[5,3] A. P. Jacob,[1] A. Mendez,[1] J. R. North,[1] E. B. Seneta[6] and P. G. Tuthill[1]

[1]*Chatterton Astronomy Department, School of Physics, University of Sydney, NSW 2006, Australia*
[2]*Planetary Science, MS 150-21, Caltech, 1200 E. California Blvd, Pasadena, CA 91125, USA*
[3]*Institute of Astronomy, Catholic University of Leuven, Celestijnenlaan 200B, 3001 Leuven, Belgium*
[4]*Department of Astrophysics, Radboud University Nijmegen, PO Box 9010, 6500GL Nijmegen, the Netherlands*
[5]*Centre for Astrophysics, University of Central Lancashire, Preston PR1 2HE*
[6]*Astrophysics Group, Cavendish Laboratory, Cambridge University, Cambridge CB3 0HE*

Accepted 2006 May 3. Received 2006 April 21; in original form 2005 December 10

ABSTRACT

The triple system HD 158926 (λ Sco) has been observed interferometrically with the Sydney University Stellar Interferometer, and the elements of the wide orbit have been determined. These are significantly more accurate than the previous elements found spectroscopically. The inclination of the wide orbit is consistent with the inclination previously found for the orbit of the close companion. The wide orbit also has low eccentricity, suggesting that the three stars were formed at the same time.

The brightness ratio between the two B stars was also measured at $\lambda = 442$ and 700 nm. The brightness ratio and colour index are consistent with the previous classification of λ Sco A as B1.5 and λ Sco B as B2. Evolutionary models show that the two stars lie on the main sequence. Since they have the same age and luminosity class (IV), the mass–luminosity relation can be used to determine the mass ratio of the two stars: $M_B/M_A = 0.76 \pm 0.04$.

The spectroscopic data have been reanalyzed using the interferometric values for P, T, e and ω, leading to revised values for $a_1 \sin i$ and the mass function. The individual masses can be found from the mass ratio, the mass function, spectrum synthesis and the requirement that the age of both components must be the same: $M_A = 10.4 \pm 1.3$ and $M_B = 8.1 \pm 1.0$ $M_\odot$.

The masses, angular semimajor axis and the period of the system can be used to determine the dynamical parallax. We find the distance to λ Sco to be 112 ± 5 pc, which is approximately a factor of 2 closer than the *Hipparcos* value of 216 ± 42 pc.

Key words: techniques: interferometric – binaries: spectroscopic – binaries: visual – stars: fundamental parameters.

1 INTRODUCTION

The bright southern star λ Scorpii (HD 158926, 6527, $\alpha_{2000} = 17^h33^m36\overset{s}{.}52$, $\delta_{2000} = -37^\circ06'13\overset{''}{.}8$, $V = 1.62$) is classified as a B2IV+B single-lined spectroscopic binary system in the Bright Star Catalogue (Hoffleit & Warren 1991), but it is in fact a triple system. Two recent papers by Uytterhoeven and colleagues (Uytterhoeven et al. 2004a,b) present a detailed spectroscopic study of the system based on 14 years of data. We will refer to these as Papers I and II. These papers also include an extensive review of the literature on λ Sco, and here we present only a brief synopsis.

The system comprises two B stars of similar mass that orbit each other with a period of approximately 1000 d (the 'wide' system). The primary is a β Cephei-type variable with a low-mass companion that orbits the primary with a period of 6 d (the 'close' system). The spectroscopic elements for the two orbits are given in Paper I. The close binary system is eclipsing, and in Paper I it is shown that this constrains the inclination to the range $70^\circ < i_{\rm close} < 90^\circ$. An independent argument in Paper II, based on frequency analysis, also gives the same result.

Paper II notes that the wide orbit cannot be accurately determined from the spectroscopy. We report here interferometric observations

⋆E-mail: W.Tango@physics.usyd.edu.au (WJT)

made with the Sydney University Stellar Interferometer (SUSI) on the wide system that results in a much improved orbit.

In Section 2, we present the SUSI observations and the new interferometric orbit.

In Section 3, the interferometric elements are used to determine a revised spectroscopic orbit. Interferometry also provides the brightness ratio between the distant component and the primary. The mass–luminosity relation can be used to find the mass ratio, and using the spectroscopically determined mass function, the individual masses can be calculated. Having determined the masses, the dynamical parallax for λ Sco can be calculated. It differs significantly from the *Hipparcos* parallax.

Following Papers I & II, we use 'close' and 'wide' to distinguish the orbital elements associated with the 6- and 1000-d periods seen in the spectrum of the primary. When no subscript is used, the wide system is implied.

In the case of the interferometric data, we follow the scheme proposed in the Washington Multiplicity Catalog (WMC) (Hartkopf & Mason 2003). The primary will be denoted by 'A', the close companion by 'a' and the wide component by 'B'. The notation a_{Aa}, for example, denotes the semimajor axis of the orbit of a relative to the primary while $a_{Aa,B}$ is the semimajor axis of B relative to the centre of light of the close pair.

2 THE SUSI OBSERVATIONS AND THE INTERFEROMETRIC ORBIT

2.1 Observations with the 'blue' beam-combining optics

Observations prior to 2004 were made at the blue wavelength of 442 nm using a bandwidth of 4 nm. The optical layout was essentially the same as the one described in Davis et al. (1999). The data were reduced using the same procedure that was employed for the analysis of the binary system β Cen (Davis et al. 2005).

Baselines of 5, 10 and 20 m were used. For these baselines, the two B stars are essentially unresolved by SUSI. Because of atmospheric turbulence, the fringe phase carries no useful information, and SUSI, like most optical interferometers, measures a quantity proportional to the squared modulus of the complex degree of coherence γ:

$$|\gamma|^2 = \frac{1+\beta^2+2\beta\cos(2\pi \boldsymbol{b}\cdot\boldsymbol{\rho}/\lambda)}{(1+\beta)^2}, \quad (1)$$

where $\boldsymbol{b}$ is the projected baseline, $\boldsymbol{\rho}$ is the vector separation between the two components of the binary as seen from the Earth and $\beta = I_B/I_A \leqslant 1$ is the brightness ratio.

The SUSI data taken with the blue beam-combining system are 'uncalibrated', i.e. no unresolved reference stars were observed to take into account the reduction in the observed fringe signal due to atmospheric and instrumental effects. The seeing conditions vary during the night, and experience has shown that modelling this by a simple linear time variation is usually adequate. We therefore assume that the observed signal will have the form

$$|V|^2 = (C_a - C_b t)|\gamma|^2, \quad (2)$$

where t is the hour angle of λ Sco. The two empirical factors, C_a and C_b, are free parameters in the model-fitting procedure. The sign in equation (2) reflects the fact that in general the seeing deteriorates during the night.

It should be noted that the cosine term in equation (1) depends on the position angle θ and the separation $\boldsymbol{\rho}$. When the raw $|V|^2$ data are fitted using equation (2), the resultant estimates for $\boldsymbol{\rho}$ and θ are not significantly affected by the fact that the data are uncalibrated.

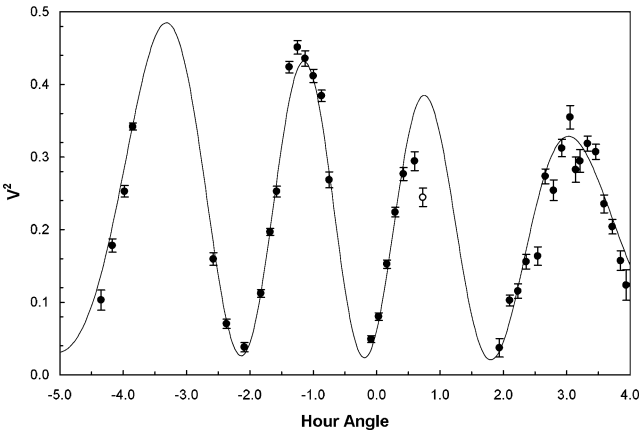

Figure 1. A typical set of data from one night (2000 June 27). Each point represents a measurement of $|V|^2$. The data are fitted using equation (2) and the best fit is shown. The error bars denote the formal errors of the data points. The actual uncertainties are estimated to be 2.8 times larger. The point shown as an open circle was omitted from the final fit.

The estimate for the brightness ratio, on the other hand, may be subject to systematic errors.

The presence of a cosine in equation (1) means that there is a 180° ambiguity in the position angle (a two-aperture interferometer cannot distinguish between $\boldsymbol{\rho}$ and $-\boldsymbol{\rho}$). This has no impact on the interpretation of the results presented here.

Equation (1) does not take into account the presence of the close binary orbiting the primary. However, Paper I notes that the contribution of H_α emission from weak T Tauri stars is at least 2 orders of magnitude fainter than the primary. Modulation due to the faint companion will be at most 1 per cent, and generally much smaller than this. This is less than the measurement noise, and consequently the effect of the T Tauri component on the interferometric data will be negligible.

The binary star measures were estimated from the $|V|^2$ data using essentially the same procedure described by Davis et al. (2005). The data from each night were fitted using equation (2), and the data for a typical night are shown in Fig. 1. The formal error for each data point in general underestimates the actual scatter because the seeing varies throughout the night. Having found the best fit to the data, the formal errors are rescaled to make $\chi^2 = \nu$, where χ^2 is the weighted sum of the squared residuals and ν is the number of degrees of freedom. In effect, we assume that the actual uncertainties obey Gaussian statistics, and all the data points are similarly affected by seeing. (In the example shown in Fig. 1, the scaling factor was 2.8.) Using the rescaled weighting factors, Monte Carlo simulation is then used to determine the uncertainties in the fitting parameters.

The assumption that all the points are equally affected by seeing is not strictly true, but if the seeing does not change dramatically during the night this assumption is, on average, realistic. The seeing is continually measured and logged, and points that are badly affected by seeing are excluded from the final fit.

A completely independent analysis was performed using simulated annealing (Kirkpatrick, Gelatt & Vecchi 1983). Simulated annealing is more likely to converge on the true minimum of χ^2 rather than on a local minimum, unlike steepest descent methods. The simulated annealing results did not differ significantly from those obtained by our standard method, and we are confident that the values of ρ, θ and β and their uncertainties that are given in Table 1 are the best fit to each night's data. The separation ρ and related quantities are all expressed in milliarcsec (mas).

Table 1. The binary star measures determined with SUSI. The date, Julian date, the baseline used and the wavelength are tabulated along with the measured values of ρ, θ, β and their uncertainties. The weighting factor W was used when fitting the orbit and is a measure of the accuracy of each point. The final column gives the residual between the observed data and the position calculated from the best-fitting model. Using the WMC nomenclature, all these observations are classified as Aa, B.

Date (UT)	JD	B (m)	λ (nm)	$\Delta\lambda$ (nm)	ρ (mas)	σ_ρ (mas)	θ	σ_θ	β	σ_β	W (mas^{-1})	$\lvert O-C\rvert$ (mas)
1999-05-15	245 1314.1	10	442	4	45.86	0.19	265.°92	0.°06	0.532	0.008	5.0	0.51
1999-05-17	245 1316.1	5	442	4	45.66	0.27	266.°37	0.°08	0.596	0.009	3.6	0.44
1999-06-04	245 1334.1	5	442	4	46.12	0.18	267.°95	0.°07	0.649	0.009	5.2	0.73
1999-06-22	245 1352.1	5	442	4	46.79	0.97	268.°93	0.°27	0.540	0.013	1.0	0.50
1999-06-23	245 1353.1	5	442	4	46.25	0.83	268.°50	0.°26	0.580	0.023	1.2	1.11
1999-08-12	245 1403.1	5	442	4	44.53	1.82	273.°09	0.°43	0.482	0.020	0.5	1.40
2000-05-11	245 1676.1	10	442	4	25.73	0.21	72.°46	0.°19	0.553	0.015	4.5	0.34
2000-05-12	245 1677.1	10	442	4	26.08	0.14	72.°73	0.°10	0.596	0.006	6.6	0.29
2000-05-15	245 1680.1	10	442	4	26.96	0.16	73.°95	0.°11	0.590	0.019	5.9	0.16
2000-05-18	245 1683.1	10	442	4	28.33	0.11	74.°74	0.°09	0.609	0.003	8.4	0.52
2000-05-27	245 1692.1	10	442	4	30.23	0.23	76.°49	0.°19	0.537	0.010	4.0	0.18
2000-06-02	245 1698.1	10	442	4	31.43	0.14	77.°56	0.°13	0.528	0.005	6.4	0.06
2000-06-03	245 1699.1	10	442	4	31.45	0.10	77.°57	0.°07	0.600	0.002	9.0	0.29
2000-06-04	245 1700.1	10	442	4	31.25	0.10	77.°72	0.°05	0.575	0.005	10.0	0.72
2000-06-07	245 1703.1	10	442	4	32.41	0.13	78.°35	0.°06	0.529	0.008	7.3	0.26
2000-06-11	245 1707.1	10	442	4	33.45	0.28	78.°83	0.°14	0.468	0.008	3.4	0.21
2000-06-27	245 1723.1	10	442	4	36.94	0.14	81.°39	0.°07	0.613	0.014	6.7	0.10
2000-06-30	245 1726.1	10	442	4	37.44	0.24	81.°83	0.°14	0.455	0.010	3.9	0.20
2000-07-01	245 1727.1	5	442	4	40.00	0.40	82.°08	0.°18	0.588	0.014	2.4	2.16
2000-07-22	245 1748.1	5	442	4	43.54	0.21	84.°10	0.°09	0.560	0.009	4.4	1.83
2000-08-02	245 1759.1	5	442	4	44.30	0.26	85.°30	0.°16	0.543	0.012	3.5	0.83
2001-06-22	245 2083.1	10	442	4	18.80	0.17	129.°16	0.°43	0.534	0.012	4.5	1.14
2001-08-10	245 2132.1	10	442	4	12.97	0.16	163.°25	1.°61	0.563	0.018	2.5	0.62
2001-08-19	245 2141.1	20	442	4	12.58	0.04	174.°46	0.°43	0.476	0.009	9.6	0.54
2004-04-15	245 3111.2	20	700	80	24.05	0.20	118.°92	0.°24	0.544	0.001	4.5	0.69
2004-04-20	245 3116.2	20	700	80	23.38	0.24	119.°37	0.°51	0.518[a]	0.028	3.1	0.34
2004-06-24	245 3181.0	20	700	80	12.77	0.03	160.°40	0.°30	0.488	0.006	13.3	0.26
2005-04-17	245 3478.2	20	700	80	47.42	0.20	270.°36	0.°05	0.516	0.014	4.8	0.18
2005-07-18	245 3570.0	15	700	80	37.83	0.37	279.°45	0.°10	0.635[a]	0.019	2.6	0.17
2005-07-21	245 3573.0	15	700	80	37.18	0.23	279.°76	0.°05	0.536[a]	0.013	4.2	0.24
2005-08-17	245 3600.0	15	700	80	32.23	0.28	283.°68	0.°07	0.543[a]	0.008	3.5	0.45

[a] $V^2_{\max} < 1$ for these sets of data. The other observations at 700 nm were fitted using $|V|^2 = 1$. This is discussed in Section 2.2.

2.2 Observations with the 'red' beam-combining optics

The more recent SUSI data have been obtained with the red beam-combining optics. This system has been described in Davis et al. (in preparation). The observations were made using baselines in the range 10–20 m. Again, the individual B stars are unresolved at these baselines and the effect of the 6-d companion on the data will be negligible.

The red observations were made at $\lambda = 700$ nm using a bandwidth of 80 nm. With such a wide bandwidth, the effects of 'bandwidth smearing' cannot be ignored. Tango & Davis (2002) have discussed bandwidth smearing in the context of single stars, and it is straightforward to generalize their results to arbitrary systems. In particular, if $\nu = c/\lambda$ is the optical frequency, S_ν is the spectral response of the interferometer and

$$N_\nu = \iint \mathrm{d}^2\boldsymbol{x} I_\nu(\boldsymbol{x}) \tag{3}$$

is the integrated monochromatic flux from the source (the integral is taken over the plane of the sky), the broad-band complex degree of coherence will be

$$\overline{\gamma} = \frac{\int_0^\infty \mathrm{d}\nu S_\nu N_\nu \gamma(\nu)}{\int_0^\infty \mathrm{d}\nu S_\nu N_\nu}, \tag{4}$$

where $\gamma(\nu)$ is the quasi-monochromatic complex degree of coherence defined by

$$\gamma(\nu) = N_\nu^{-1} \iint \mathrm{d}^2\boldsymbol{x} \exp\{-2\pi i \boldsymbol{b}\cdot\boldsymbol{x} c^{-1}\nu\} I_\nu(\boldsymbol{x}). \tag{5}$$

The complex coherence $\gamma(\nu)$ will vary with frequency (i) because of the frequency dependence of the Fourier kernel and (ii) because $I_\nu(\boldsymbol{x})/N_\nu$ is also a function of the frequency. In the case of a binary system with unresolved components, this latter effect will be unimportant.

We assume that the bandwidth is rectangular, having a width $\delta\nu$ centred on ν_0. Let $\lambda_0 = c/\nu_0$ and make the usual approximation that $\delta\nu \approx c\delta\lambda/\lambda_0^2$. For convenience define $\psi = 2\pi\boldsymbol{b}\cdot\boldsymbol{\rho}/\lambda_0$. The equivalent of equation (1) including bandwidth smearing becomes

$$|\gamma|^2 = \frac{1 + \beta^2\ \mathrm{sinc}^2(\psi\delta\lambda/2\lambda_0) + 2\beta\ \mathrm{sinc}(\psi\delta\lambda/2\lambda_0)\cos\psi}{(1+\beta)^2}. \tag{6}$$

In the case of λ Sco, the effect of bandwidth smearing can reduce $|\gamma|^2$ by several per cent. The effect is time-dependent, and is most significant when $\boldsymbol{b}$ and $\boldsymbol{\rho}$ are parallel.

The red table observations were first processed using the 'data pipeline' described in Davis et al. (in preparation). The output is a set of calibrated measures of $|V|^2$. The visibility measures for each

night were fitted using the same procedure adopted for the 'blue' observations. The only difference is that the red data are fitted using equation (6) rather than equation (2). The most notable difference between the blue and red data sets is that the errors in the red data points required very much less rescaling, confirming the fact that the use of calibrators significantly reduces the effects of seeing on the data.

If the data are properly calibrated, the maximum value of $|V|^2$, $|V|^2_{\rm max}$, should be 1. On several nights, however, it was found that allowing $|V|^2_{\rm max}$ to be a free parameter gave significantly better fits, with $|V|^2_{\rm max} < 1$. The reduction cannot be explained by the partial resolution of the B stars or the modulation caused by the 6-d close companion. We believe that the effect is most likely instrumental, but there are as yet not enough data to establish the exact cause. This effect has a negligible effect on the values of ρ and θ, but may affect β.

The results from the observations made with the red beam-combining system are given in Table 1.

2.3 The interferometric orbit

The orbital elements were calculated, again using the same procedure that was employed for β Cen (Davis et al. 2005). Each measure in Table 1 was given a weight according to the formula: $W = (\sigma_\rho^2 + \rho^2\sigma_\theta^2)^{-1/2}$. The results are given in Table 2, and the '$|O - C|$' residuals are tabulated in Table 1.

The uncertainties in the orbital elements were estimated using Monte Carlo simulation using the best-fitting orbital elements and the weighting factors in Table 1 to generate the simulated data sets. The resultant uncertainties are also listed in Table 2.

The period P, epoch of periastron T and eccentricity e differ significantly from those given in Paper I (see Table 3), and we return to this in Section 3.

The computed orbit and the observed measures are shown in Fig. 2. This figure also confirms the fact that any effects caused by the close companion must be smaller than the fitting errors.

Our value of the inclination, $i_{Aa,B} = 77\overset{\circ}{.}2 \pm 0\overset{\circ}{.}2$, is completely consistent with the range $70^\circ \leqslant i_{\rm close} \leqslant 90^\circ$ given in Papers I and II and, together with the relatively low eccentricity of the interferometric orbit, supports the hypothesis that the B component did not join the system as a result of a tidal capture event.

Table 2. The orbital elements of λ Sco determined from the SUSI observations. All the elements refer to the Aa,B orbit.

Element	Value, uncertainty and units	
P	1052.8 ± 1.2	d
T	$51\,562.3 \pm 2.8$	MJD
e	0.121 ± 0.005	
a''	49.3 ± 0.3	mas
i	$77\overset{\circ}{.}2 \pm 0\overset{\circ}{.}2$	
ω	$74\overset{\circ}{.}8 \pm 0\overset{\circ}{.}9$	See note
Ω	$271\overset{\circ}{.}30 \pm 0\overset{\circ}{.}15$	
$(a'')^3/P^2$	$(108 \pm 2) \times 10^{-12}$	asec^{3}d^{-2}

Note: This is the argument of periastron for the orbit of the B component relative to the primary. The corresponding quantity in Table 3 refers to the orbit of the primary around the system barycentre. The two angles differ by 180°.

Table 3. The second column lists the elements found in Paper I using the FOTEL code. The third column tabulates the elements used in the final fit: P, T, e and ω are based on the SUSI; K has been recomputed using these values. The uncertainties are the formal uncertainties of the fit and do not include systematic effects.

Element	FOTEL	FOTEL+SUSI
P (d)	1082 ± 3	1052.8 ± 1.2
K (km s^{-1})	24.7 ± 0.4	22.8 ± 0.4
T (MJD)	$51\,731.5 \pm 29$	$51\,562.3 \pm 2.8$
e	0.23 ± 0.03	0.121 ± 0.005
ω	$311^\circ \pm 11^\circ$	$254\overset{\circ}{.}8 \pm 0\overset{\circ}{.}9$

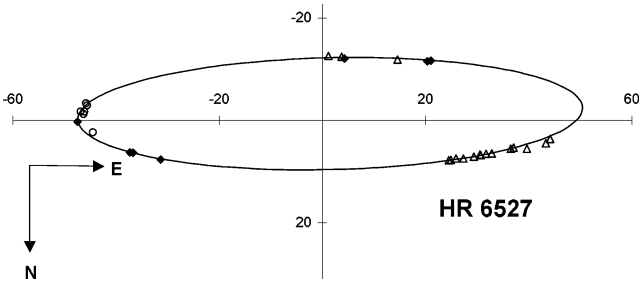

Figure 2. The orbit of λ Sco. The scale is in milliarcsec and the orientation conforms to standard practice (Heintz 1978). Different symbols are used to denote successive orbits, referred to the epoch of periastron T. The circles indicate data taken in 1999. The triangles are the data from 2000 and 2001. The diamonds denote points on the next orbit during 2004 and 2005. Open symbols are used for observations at 442 nm, and filled symbols denote 700-nm observations.

2.4 The brightness ratio and the mass ratio

For the reasons discussed in Section 2.1, the brightness ratio β is subject to systematic errors associated with the way the $|V|^2$ data are normalized. As well, the system is a β Cephei variable with a photometric amplitude in v of approximately 0.023 mag and a period of 5.1 h (Shobbrook & Lomb 1972, 1975).

Shobbrook & Lomb (1975) also observed periodic variations in colour. The amplitudes of the variation were $(b - v) = 0.002 \pm 0.001$ and $(u - b) = 0.0098 \pm 0.0012$.

The measured brightness ratios and their uncertainties are plotted in Fig. 3. The data fall into two groups: the earlier set of points were observed using $\lambda = 442$ nm while the more recent set was obtained using $\lambda = 700$ nm. The two lines represent the approximate spread in β that would be expected from the intrinsic variability ($\sim\pm0.012$ mag). The error bars indicate the statistical uncertainties for each observation, but in the present context they are misleading, since there are significant night-to-night variations due to the intrinsic variability of λ Sco as well as the instrumental effects (calibration errors) previously discussed. In our view, the average and standard error of the blue and red data sets represent the best estimates of the brightness ratios.

The mean and standard deviations for the brightness ratio for each set, and the corresponding magnitude differences, are

$$\beta_{442} = 0.55 \pm 0.05 \qquad \Delta m_{442} = 0.65 \pm 0.10 \tag{7}$$

$$\beta_{700} = 0.54 \pm 0.05 \qquad \Delta m_{700} = 0.67 \pm 0.10. \tag{8}$$

The difference in the colour index $(m_{442} - m_{700})$ between λ Sco A and B is -0.02 ± 0.14. Both the magnitude and colour index

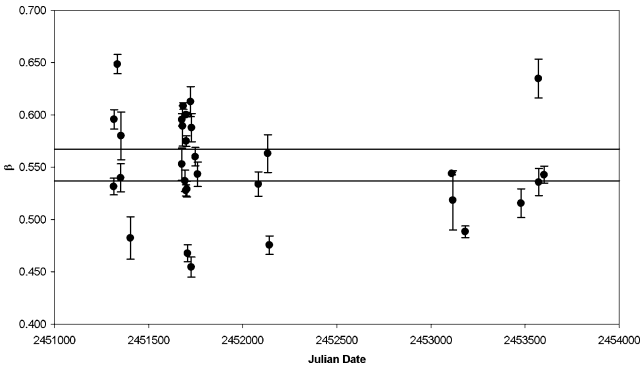

Figure 3. The brightness ratios taken from Table 1. The two lines denote the range in β that is expected due to the intrinsic variability of the system. The data prior to JD 245 2500 were measured at $\lambda = 442$ nm. The more recent data were measured at 700 nm.

differences are consistent with the relative spectral classification of λ Sco A as B1.5 IV and λ Sco B as B2 V given in Paper I.

Although the A and B components have apparently different luminosities, due to the complexity of this system and the fast rotation there is an uncertainty of up to 0.2 dex in $\log g$, making it difficult to establish the luminosity class with certainty. However, the inclination of the long period orbit suggests that the three stars formed together and λ Sco A and B are thus both on the main sequence. The brightness ratio then implies that the effective temperatures can be fixed at 25 000 and 21 000 K. The contribution of the T Tauri star to the luminosity of the primary is negligible and the empirical mass–luminosity relation $\log(L_B/L_A) = (3.51 \pm 0.14)\log(M_B/M_A)$ (Griffiths, Hicks & Milone 1988) can be used to find the mass ratio for λ Sco A and B. The ratio of the luminosities has been obtained from the V magnitude difference, taken to be 0.66 ± 0.10 by interpolation between Δm_{442} and Δm_{700}, and the difference in bolometric correction (BC). The latter has been obtained from interpolation in the tables by Flower (1996) for main-sequence B stars. Assuming an uncertainty of ±1000 K in the effective temperatures as obtained in Paper I, we arrive at $(\mathrm{BC}_A - \mathrm{BC}_B) = -0.40 \pm 0.10$. Thus, the mass ratio for λ Sco A and B is

$$\frac{M_B}{M_A} = 0.76 \pm 0.04. \quad (9)$$

This is consistent with the value of $M_B/M_A = 0.84 \pm 0.12$ estimated from the spectrum synthesis analysis presented in Paper I.

3 THE COMBINED INTERFEROMETRIC AND SPECTROSCOPIC ORBIT

The spectroscopic orbital elements were determined in Paper I using two different codes, FOTEL and VCURVE. The upper panel of Fig. 4 plots the radial velocity (RV) data against the FOTEL phase. The solid line is the calculated RV using the FOTEL elements (This panel is the same as the lower panel in fig. 2 of Paper I.).

The interferometric values for P, T, e and ω are much more accurate than the spectroscopically determined ones, and the original RV data were refitted using these values, giving $K_{\mathrm{wide}} = 22.8 \pm 0.4\,\mathrm{km\,s^{-1}}$. Table 3 tabulates the elements given in Paper I and our revised values, and the RV amplitude calculated using these elements is shown in the lower panel of Fig. 4.

Some words of caution on the accuracy of the RV data are in order. The use of two types of spectra of very different nature and quality forced the authors of Paper I to use different methodology

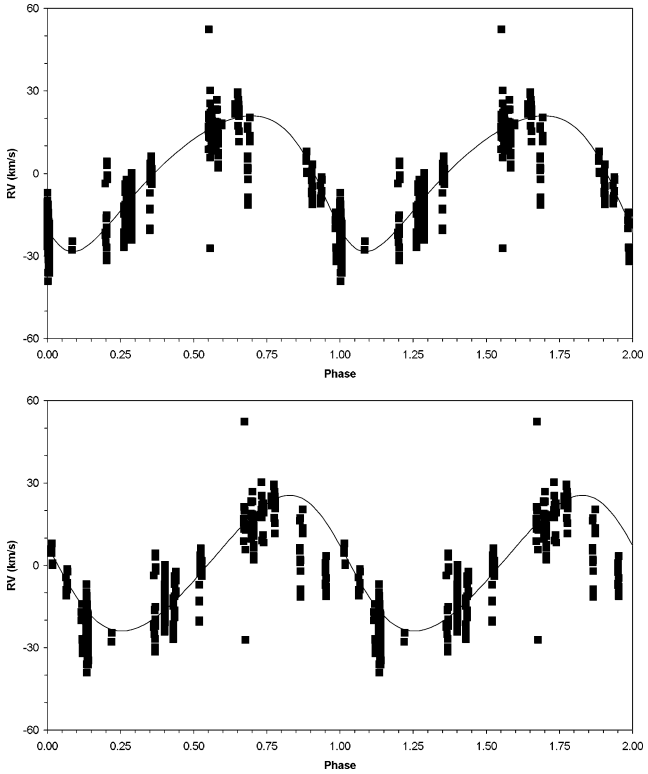

Figure 4. The RV data for the 'wide' system in λ Sco. The RV due to the 'close' system has been removed. In the upper panel, the data are plotted against the FOTEL phase and the RV curve is calculated from the FOTEL elements in Table 3. The same RV data are plotted in the lower panel against the SUSI phase, with the RV curve calculated using the elements given in the final column of Table 3.

to derive the RV values. In doing so, they ignored the fact that the B component contributes to the spectral lines used for the RV computation, given that the binary is observed to be single-lined. The light, and hence mass ratio, found from the interferometry is an order of magnitude more precise than the one in Paper I and thus allows us to place better constraints on the individual masses of the A and B components. The ranges listed in Paper I must be revised, as they do not include the systematic effects due to the B component on the spectral lines used to determine the amplitude of the RV.

To make the best use of the interferometric results, it is important to understand the uncertainties and possible systematic effects in the RV data. In general, the contribution of the B component to the lines leads to an underestimation of the RV of the primary. As a consequence, the derived quantities $a \sin i$ and the mass function are also underestimated. This fact was clearly demonstrated and corrected for by spectral disentangling in the case of the double-lined binary β Cen (Ausseloos et al. 2006), where it implied a 10 per cent increase in the individual component masses. We are unable to apply such a treatment to λ Sco because the disentangling fails in this single-lined case with three stellar components, of which at least one is oscillating (see Paper II). Nevertheless, we can estimate the systematic errors of the RVs for the two sets of data from which they were derived:

(i) the high signal-to-noise ratio (S/N) single-order spectra including the Si III 4553Å line taken with the Coudé Echelle Spectrograph on the Coudé Auxilliary Telescope (CAT/CES);
(ii) the low S/N échelle spectra taken with Euler/CORALIE.

The resolution for both sets of data is nearly the same (see Paper I for further details).

From set (i), we derive that the lines due to the B component are completely situated within those of the primary (see Paper I and Waelkens 1990 for appropriate plots of the lines). Moreover, from the brightness ratio and the temperature ranges listed in Paper I, we derive that the λ Sco B contributes 40 per cent to the total equivalent width of the Si III line used to determine the RVs. This places strong constraints on the upper limit to $K_{\rm wide}$: the fact that the B component is not seen in the wings of the high-quality CAT profiles implies that $K_{\rm wide} < 25.7\,{\rm km\,s^{-1}}$ (which we deduce from merging the contributions of the two stars to the Si III line with the appropriate equivalent width (EW) ratios and $v \sin i$ estimates of Papers I and II). This suggests a conservative range for $K_{\rm wide}$ is $[22.4, 25.7]\,{\rm km\,s^{-1}}$. Table 4 tabulates the system parameters that are affected by the uncertainties in the RV amplitude. The accurate value of the mass ratio given in equation (9) has been used to calculate the individual masses from the mass function.

The mass ranges listed in Table 4, although compatible with those given in Paper I, are very broad. We tried to constrain them further by taking into account the results from the spectrum synthesis presented in Paper I, in which the contributions from the individual components were properly taken into account to fit H, He and Si lines in data set (ii). We did this by scanning the data base of standard stellar evolution models computed by Ausseloos et al. (2004). We selected models from the zero-age main sequence (ZAMS) to the terminal-age main sequence (TAMS) with $X = 0.70$ and Z in the range 0.012 to 0.030. Models with the three values, 0.0, 0.1 and 0.2, for the core overshooting parameter (expressed in units of the local pressure scaleheight) were included. While scanning the data base, we required that the two stars not only satisfy the mass ranges given in Table 4, but also have the appropriate luminosity ratio given by the interferometry, and have $\log T_{\rm eff}$ and $\log g$ in the ranges found from the spectrum synthesis done in Paper I. Moreover, we required that their ages be the same to within 0.1 per cent (following the interferometric result that the orbital inclinations of the A and B components are consistent with each other). In this way, we find the acceptable range for the mass of the primary M_A to be [9.0, 11.7] $M_\odot$ and the range for M_B to be [7.0, 9.1] $M_\odot$.

All the acceptable model combinations at the lower mass ends of these intervals have an age below 10^7 yr corresponding to less than 60 per cent of the main-sequence lifetime, while those at the upper mass end correspond to an age below 13×10^7 yr which is less than 30 per cent of the main-sequence duration. For the lower mass end, this is consistent with the suggestion made in Paper I that λ Sco contains a pre-MS star. Indeed, from Palla & Stahler (1993) we note that a pre-MS star with a mass of $\sim$1.5 $M_\odot$ remains about 10^7 yr in its pre-MS stage when a B-type star formed from the same accretion disc has reached the ZAMS. Table 5 summarizes our conclusions regarding the three components of λ Sco.

Table 4. System parameters that depend on the RV amplitude. The lower limit for $K_{\rm wide}$ is taken from Table 3. The upper limit is based on our best estimates of the effects of the wide component on the RV data and from the interferometric data.

Element	Range	
$K_{\rm wide}$	[22.4, 25.7]	km s^{-1}
$a_1 \sin i_{\rm wide}$	[2.15, 2.47]	AU
a_1	[2.21, 2.53]	AU
$f(M)$	[1.20, 1.82]	$M_\odot$
M_A	[9.39, 14.25]	$M_\odot$
M_B	[7.05, 10.69]	$M_\odot$

Table 5. Summary of the stellar parameters of the three components of λ Sco. The mass of the component is taken from Paper I; the masses of λ Sco A and B are based on the work presented here (compare with table 4 of Paper I).

	Mass ($M_\odot$)	$T_{\rm eff}$ (K)	$\log g$	
A	10.4 ± 1.3	$25\,000 \pm 1000$	3.8 ± 0.1	B1.5 IV
a	1.8 ± 0.2			pre-MS
B	8.1 ± 1.0	$21\,000 \pm 1000$	4.0 ± 0.1	B2 IV

3.1 The dynamical parallax

The dynamical parallax is

$$\pi_d = \frac{365.25^{2/3}}{(M_{Aa} + M_B)^{1/3}} \left[\frac{(a'')^3}{P^2}\right]^{1/3}, \qquad (10)$$

where M_{Aa} is the combined mass of the primary (A) and the close companion (a) and M_B the mass of the B component. We have used the estimates given in Table 5 and the interferometric value of $(a'')^3/P^2$ (Table 2) to find the distance to λ Sco:

$$D = 1/\pi_d = 112 \pm 5{\rm pc}. \qquad (11)$$

Our distance is smaller than the *Hipparcos* value of 216 ± 42 pc (Perryman et al. 1997) by nearly a factor of 2 (i.e. 2.5 times the *Hipparcos* standard deviation). It has been noted (de Zeeuw, Hoogerwerf & de Bruijne 1999) that the motion in binary systems can significantly bias *Hipparcos* parallaxes and a similar phenomenon has been observed with β Cen (Davis et al. 2005).

The revised parallax may have implications regarding the membership of λ Sco in the Scorpius–Centaurus–Lupus–Crux complex of OB associations. Brown & Verschueren (1997) suggested that it was a member of the Upper Scorpius (US) association, but de Zeeuw et al. (1999) did not include λ Sco as a secure member of the US association based on an analysis of *Hipparcos* positions, parallaxes and proper motions. The revised parallax corresponds to the Lower Centaurus Crux (LCC) association, which lies at a distance of 116 ± 2 pc. The Galactic coordinates of λ Sco, however, still exclude it as a definite member of the association.

4 SUMMARY

Observations with SUSI have been used to establish an interferometric orbit for λ Sco. The accuracy of the period, epoch of periastron, eccentricity and argument of periastron are significantly better than those previously found (Paper I). We have combined the interferometric and spectroscopic elements to provide an orbital solution which is consistent with both the interferometric and spectroscopic data. The inclination of the orbit for the wide component is consistent with that previously found for the close companion, and the eccentricity of its orbit is quite low. This is strong evidence that the system was formed from a common accretion disc rather than through tidal capture.

The brightness ratio allows the mass ratio of the two B stars to be estimated from the mass–luminosity relation. The estimated mass ratio of 0.76 ± 0.04 agrees with the masses determined by the synthetic spectrum analysis presented in Paper I. The limiting

factor in the determination of the individual masses and the semi-major axis is clearly the large uncertainties of the RV values. This is due to our inability to disentangle the contributions of the primary and wide companion to the lines in the overall spectrum. While sophisticated disentangling methodology is available in the literature, e.g. Hadrava (1995), its application to single-lined binaries has not yet been achieved to our knowledge. In the case of λ Sco, the β Cep oscillations are an additional factor that complicates the disentangling. Nevertheless, we have taken a conservative approach to estimate the mass ranges from the spectroscopic orbital RV, and we have constrained them further from spectrum synthesis results and from requiring equal ages and the appropriate brightness ratio from the SUSI data. In this way, we obtained a relative precision of about 12 per cent for the masses of both λ Sco A and B. Masses of B-type stars are not generally known to such a precision.

Accurate mass estimates of pulsating massive stars are important for asteroseismic investigations of these stars. Indeed, the oscillation frequencies of well-identified modes in principle allow the fine-tuning of the physics of the evolutionary models [see Aerts et al. (2003) for an example]. For this to be effective when only a few oscillation modes have been identified, we need an independent high-precision estimate of the effective temperature and of the mass of the star. This is generally not available for single B stars. The λ Sco Aa system is one of the bright close binaries with a β Cep component, and it is only the second one, after β Cen, for which a full coverage of the orbit with interferometric data is available. The results presented in this paper therefore constitute a fruitful starting point for seismic modelling of the primary of λ Sco, particularly now that the *Wide-Field Infrared Explorer* (*WIRE*) satellite has provided several more oscillation frequencies compared to those found in Paper II (Bruntt & Buzasi, private communication).

The mass estimates, when combined with the period and angular semimajor axis found from the interferometric orbit, allow the dynamical parallax to be calculated. We find the distance to the λ Sco system of 112 ± 5 pc, which is almost a factor of 2 smaller than the *Hipparcos* distance of 216 ± 42 pc. The reason for the large discrepancy is almost certainly due to the B component since it is of comparable brightness to the primary, and the orbital period is approximately 3 yr. The fact that many of the B stars in the Sco–Cen association are multiple systems suggests that the *Hipparcos* parallaxes for these stars must be used with care.

ACKNOWLEDGMENTS

This research has been carried out as a part of the SUSI project, jointly funded by the University of Sydney and the Australian Research Council.

MJI acknowledges the support provided by an Australian Postgraduate Award; APJ acknowledges the support of a Denison Postgraduate Award from the School of Physics and JRN acknowledges the support of a University of Sydney Postgraduate Award.

CA and KU are supported by the Fund for Scientific Research of Flanders (FWO) under grant G.0332.06 and by the Research Council of the University of Leuven under grant GOA/2003/04.

REFERENCES

Aerts C., Thoul A., Daszyńska J., Scuflaire R., Waelkens C., Dupret M.-A., Niemczura E., Noels A., 2003, Sci, 300, 1926
Ausseloos M., Scuflaire R., Thoul A., Aerts C., 2004, MNRAS, 355, 352
Ausseloos M., Aerts C., Lefever K., Davis J., Harmanec P., 2006, A&A, in press
Brown A. G. A., Verschueren W., 1997, A&A, 319, 811
Davis J., Tango W. J., Booth A. J., ten Brummelaar T. A., Minard R. A., Owens S. M., 1999, MNRAS, 303, 773
Davis J. et al., 2005, MNRAS, 356, 136
de Zeeuw P. T., Hoogerwerf R., de Bruijne J. H. J., 1999, AJ, 117, 354
Flower P. J., 1996, ApJ, 469, 355
Griffiths S. C., Hicks R. B., Milone E. F., 1988, J. R. Astron. Soc. Canada, 82, 1
Hadrava P., 1995, A&AS, 114, 393
Hartkopf W. I., Mason B. D., 2003, XXVth General Assembly of the IAU, Special Session 3 (abstract only)
Heintz W. D., 1978, Double Stars. Reidel, Dordrecht
Hoffleit D., Warren W. H., 1991, The Bright Star Catalogue. 5th Revised edn, Astronomical Data Center, NSSDC/ADC
Kirkpatrick K., Gelatt C. D., Vecchi M. P., 1983, Sci, 220, 671
Narayanan V. K., Gould A., 1999, ApJ, 523, 328
Palla F., Stahler S. W., 1993, ApJ, 418, 414
Perryman M. A. C., Lindgren L., Kovalevsky J. et al., 1997, A&A, 323, L49
Shobbrook R. R., Lomb N. R., 1972, MNRAS, 156, 181
Shobbrook R. R., Lomb N. R., 1975, MNRAS, 178, 709
Tango W. J., Davis J., 2002, MNRAS, 333, 642
Uytterhoeven K., Willems B., Lefever K., Aerts C., Telting J. H., Kolb U., 2004a, A&A, 427, 581 (Paper I)
Uytterhoeven K., Telting J. H., Aerts C., Willems B., 2004b, A&A, 427, 593 (Paper II)
Waelkens C., 1990, Angular Momentum and Mass Loss for Hot Stars. Proceedings of the Advanced Research Workshop D. Reidel, Dordrecht, p. 235

This paper has been typeset from a TEX/LATEX file prepared by the author.